Sex Plant Reprod (2011) 24:47–61
DOI 10.1007/s00497-010-0147-7

ORIGINAL ARTICLE

The cytohistological basis of apospory in *Hypericum perforatum* L.

G. Galla · G. Barcaccia · A. Schallau · M. Puente Molins · H. Bäumlein · T. F. Sharbel

Received: 12 March 2010 / Accepted: 12 June 2010 / Published online: 2 July 2010

Abstract St. John's wort (*Hypericum perforatum* L., $2n = 4x = 32$) is a medicinal plant that produces pharmaceutically important metabolites with antidepressive, anticancer and antiviral activities. It is also regarded as a serious weed in many countries. *H. perforatum* is furthermore an attractive model system for the study of apomixis**.** Natural populations of *H. perforatum* are predominantly composed of tetraploid individuals, although diploids and hexaploids are known to occur. It has been demonstrated that while diploids are sexual, polyploids are facultative apomictic whereby a single individual can produce both sexual and apomictic seeds. Despite our increasing understanding of gamete formation in sexually reproducing species, relatively little is known regarding the cytological basis of reproduction in *H. perforatum*. Here, we have studied embryo sac formation and the genetic constitution of seeds by means of staining-clearing of ovules/ovaries, DIC microscopy and flow cytometric seed screening (FCSS) of embryo and endosperm DNA contents. Comparisons of female sporogenesis and gametogenesis between sexual and apomictic accessions have enabled the identification of major phenotypic differences in embryo sac formation, in addition to complex fertilization scenarios entailing reduced and unreduced male and female gametes. These data provide new insights into the production of aposporous seeds in *H. perforatum*, and complement ongoing population genetic, genomic and transcriptomic studies.

Keywords Apomixis · Apospory · Hypericum · Endosperm · Polyploid

Communicated by Thomas Dresselhaus.

G. Galla · G. Barcaccia
Department of Environmental Agronomy and Crop Science, Laboratory of Plant Genetics and Genomics, University of Padova, Campus of Agripolis—Viale dell'Università 16, 35020 Legnaro, Italy

A. Schallau · H. Bäumlein
Gene Regulation Group, Department of Molecular Genetics, Leibniz-Institut für Pflanzengenetik und Kulturpflanzenforschung (IPK), 06466 Gatersleben, Germany

G. Galla · M. Puente Molins · T. F. Sharbel (✉)
Apomixis Research Group, Department of Cytogenetics and Genome Analysis, Leibniz-Institut für Pflanzengenetik und Kulturpflanzenforschung (IPK), Corrensstraße 3, 06466 Gatersleben, Germany
e-mail: sharbel@ipk-gatersleben.de

Introduction

Sexual reproduction (amphimixis) in angiosperms is characterized by the development and fusion of highly specialized gametes originating from sporophytic parental tissues. Both male and female gametophytes are derived from specific cells through a coordinated series of events, including the meiotic production of reduced spores (sporogenesis) and their further development into pollen grains and embryo sacs through unconventional mitotic divisions (gametogenesis). In contrast, many plants reproduce through apomixis, a naturally occurring form of asexual reproduction through seed whereby offspring are genetic clones of the mother plant (Nogler 1984). It is largely believed that expression of apomixis requires the coordination of three independent mechanisms: (1) production of an unreduced embryo sac (apomeiosis); (2) the autonomous development of the embryo in the absence of fertilization (parthenogenesis) and (3) the formation of a functional endosperm (Mogie 1992; Bicknell and Koltunow

2004). Apomictic seed production can differ among species, and depending on the specific site where apomictic embryo sac differentiation takes place, gametophytic apomixis can be divided into either diplosporous or aposporous forms, the latter being characterized by the development of functional embryo sacs from somatic cells (aposporous initial, AI cells) belonging to the distal area of the ovule (Koltunow et al. 1998). Our understanding of the cytological and molecular basis of both sporogenesis and gametogenesis has been advanced by studies in different model systems, including *Arabidopsis* (Smyth et al. 1990; Mansfield et al. 1991; Robinson-Beers et al. 1992; Schneitz et al. 1995; Christensen et al. 1997) and maize (Huang and Sheridan 1994), which have shown that normal embryo sac development requires the coordinated progression of sporogenic cell specification and meiosis (Sheridan et al. 1999), followed by functional megaspore selection and mitosis to yield a functional embryo sac. Furthermore, a considerable body of information related to the genetic control and cytological development of major aposporous features has been generated from different genera including: *Hieracium* spp. (Koltunow et al. 1998; Tucker et al. 2001), *Poa pratensis* (Matzk 1991; Barcaccia et al. 1998; Albertini et al. 2001), *Brachiaria decumbens* (Pessino et al. 1997) and *Pennisetum squamulatum* (Ozias-Akins et al. 1993, 1998; Gustine and Sherwood 1997; Roche et al. 1999).

The first cytological investigations into *Hypericum perforatum* ovule and embryo sac development were published in the pioneer works of Noack (1939, 1941), Davis (1966), and more recently by Martonfi et al. (1996a). In recent years, a number of papers have been published on this species (Mártonfi et al. 1996b; Koperdakova et al. 2004), and the adoption of *Hypericum perforatum* as a model species for the study of aposporous apomixis has been proposed (Matzk et al. 2001; Barcaccia et al. 2007). This species, with a basic chromosome number of 8, is characterized by a relatively small genome size ($1C = 0.650$ pg $\approx$ 630 Mbp; Bennett and Smith 1976). Natural populations of *H. perforatum* are composed mostly of tetraploids, although diploids and hexaploids are known to occur (Matzk et al. 2001; Robson 2002). As reported by Matzk et al. (2001), apomictic (polyploid) individuals can facultatively produce both sexual and apomictic seeds. Apomictic seed production is highly variable in this species and is characterized by complex fertilization scenarios between reduced and unreduced male and female gametes (Matzk et al. 2001). Furthermore, *H. perforatum* shows a number of traits characteristic of hybridity, including variability in morphology and chemical compound production, meiotic abnormalities (e.g., lagging chromosomes), elevated pollen grain sterility, parthenogenic development of unreduced egg cells and pseudogamy (Matzk et al. 2001; Barcaccia et al. 2001).

Recent development of proteomic, genomic and transcriptomic dimensions of research, along with a continuous setting of micro-technologies such as laser micro dissection, requires a fine and detailed knowledge of case studies. Since the publication of Noack dated 1941 and despite our increasing understanding of processes related to sexual reproduction, still relatively little is known regarding the molecular and cytological basis of apomixis in *H. perforatum*. In particular, it remains unclear which somatic cells undergo a change in cell fate to become aposporic initial cells, not to mention how this process is initiated and controlled. Furthermore, it is unclear whether developing sexual and aposporous structures of *H. perforatum* undergo any form of communication. Our ultimate goal is the elucidation of the molecular genetic mechanisms leading to apomictic seed production in *H. perforatum*, and hence a clear understanding of embryological differences with normal sexual seed production is essential for subsequent "-omics" approaches. We thus present a detailed phenotypic analysis of female sporogenesis and gametogenesis in both sexual and apomictic *H. perforatum,* in addition to considering variation in these traits with respect to population origins.

Materials and methods

Plant materials

Hypericum perforatum L. plants, up to 8 individuals per genotype, for a single diploid ($2n = 2x = 16$), 4 naturally occurring tetraploids and 4 induced tetraploids ($2n = 4x = 32$), were used for all cytological experiments (Table 1). Plants of the diploid sexual line R1 (reselected from the tetraploid apomictic cultivar 'Topaz') were converted to autopolyploids by colchicine application, as follows. Seeds were imbibed in water for 24 h, placed on filter paper soaked with an aqueous solution of 0.2% colchicine for 24 h and then planted in soil for germination. The C0 plants that survived this treatment were self-pollinated, and their progenies (C1) were screened for tetraploid plants. Sexual tetraploid C1 and C2 plants were used for further crosses with tetraploid apomictic pollinators.

Flow cytometric screening of *H. perforatum* seeds

We used a flow cytometric seed screen (FCSS; Matzk et al. 2001) to measure the reproductive mode of all *H. perforatum* accessions (Table 1), using a high-throughput method developed in our laboratory. A total of 50 single seeds per accession were ground in a 96-deep well plate with 80 µl of grinding buffer (citric acid monohydrate 0.1 M, Tween 20 0.5%, pH adjusted to 2–3 and ß-mercaptomethanol) and 3 metal ball bearings (3 mm diameter) in a GenoGrinder 2000

Table 1 Geographic origin and flow cytometric characterization of the degree of apomixis for *H. perforatum* used in embryological analyses

Plant	Origin	Ploidy	Apomixis[a] (%)
H06_1915	Iron Mountain MI (USA)	4*x*	89
H06_2751	Bolzano, Italy	4*x*	69
H06_2849	Badia Polesine, Italy	4*x*	82
H06_2974	Cerbere, France	4*x*	75
322 ($F1_1$ × An)	IPK-Gatersleben[b]	4*x*	42
349 ($F_1$1 × No)	IPK-Gatersleben[b]	4*x*	31
H06_2842	Badia Polesine, Italy	2*x*	0
222 ($R1C_2$ × Si)	IPK-Gatersleben[b]	4*x*	0
29 ($F1_2$ × An)	IPK-Gatersleben[b]	4*x*	0
36 ($F1_2$ × An)	IPK-Gatersleben[b]	4*x*	0
325 ($F1_1$ × An)	IPK-Gatersleben[b]	4*x*	0
982 ($R1C_1$ × To)	IPK-Gatersleben[b]	4*x*	0
405 ($F_1$2 × An)	IPK-Gatersleben[b]	4*x*	0
407 ($F_1$2 × No)	IPK-Gatersleben[b]	4*x*	0

[a] As measured using flow cytometric seed screen (Matzk et al. 2001)

[b] Induced tetraploid plants via colchicine treatment of seeds (see "Materials and methods")

homogenizer (Spex Certiprep) at 50 strokes/sec for 2 min. After grinding, 250 µl of staining buffer (Na_2HPO_4, 12 H_2O, 0.4 M, 2 ml of DAPI solution, pH adjusted to 8.5) was added to each sample, and the obtained suspension (160 µl out of the total) filtered through a 30-µm mesh width nylon tissue. A total of 80 µl of the filtrate was then transferred into a new 96-well plate, and 80 µl of staining buffer was added to each sample. The fluorescence intensity of DAPI-stained nuclei was determined using the a Ploidy Analyser PA II hooked up to a Robby-Well autoloader (Partec GmbH, Münster, Germany), and the flow cytometric profile of each seed sample was evaluated for embryo and endosperm DNA content by using the Flomax software (Partec GmbH).

Cytohistological observations of sporogenesis and gametogenesis

Flower buds were sampled at different developmental stages, according to their length, and divided into a total of eight stages. For the length of the flower bud, the distance between the insertion point of the external carpels to the receptacle and the apex of the flower bud was considered. Flower buds ranging from a minimum of 4 mm to a maximum length of 12 mm were analyzed for each plant. Pistils were dissected from flower buds using a Zeiss Discovery.V20 (Carl Zeiss MicroImaging, Germany) stereomicroscope prior to subsequent staining procedures. Ovules were subsequently dissected onto a microscope slide and cleared with chloral hydrate/water/glycerol (8:2:1) prior to observation. Pistils were alternatively cleared and stained following the protocol reported by Stelly et al. (1984) with some minor modifications. Briefly, the tissues were fixed in FAA (3.7% formalin, 5% acetic acid, 50% ethanol) overnight at 4°C and then hydrated in 50, 75 and 100% progressive water/ethanol solutions for 30 min each. Samples were stained with pure Mayer's hemalum for 48 h, placed in 2% acetic acid for 24 h and then dehydrated in 25, 50, 70, 95 and 100% progressive ethanol solutions for 40 min each. After dehydration, samples were cleared with absolute ethanol/methyl salicylate solutions (2:1 and 1:2, v/v) and twice with pure methyl salicylate (10 min per step). Ovules were then mounted under a coverslip in one drop of pure methyl salicylate. Cytohistological observations were made using a Zeiss Axioplan (Carl Zeiss MicroImaging, Germany) microscope under DIC optics, using a 100× objective.

Decolorized aniline blue (DAB; 0.005% w/v) was used to detect the presence of callose, as described by Worrall et al. (1992). Ovules were dissected from fresh pistils directly into DAB/glycerol (1:1, w/v) under a Zeiss Discovery.V20 (Carl Zeiss MicroImaging, Germany) stereomicroscope. After ovule isolation, samples were coverslipped and observed under UV light using a Zeiss Axioplan (Carl Zeiss MicroImaging, Germany) microscope with a 365–400 nm filter set.

Synchrony of gametophyte development

To determine the extent to which female gametophyte development is synchronous within a pistil, over 50 flower buds were harvested at different developmental stages, ranging from 4 to 12 mm in length. For each flower bud, pistils were dissected from the flower and processed as reported in section "Cytohistological observations of sporogenesis and gametogenesis". Using this approach, about 1,800 ovules were isolated from different pistils and studied. A minimum number of 20 randomly selected ovules were considered for each pistil. The observed developmental stages were classified according to Schneitz et al. (1995) and counted. Statistical analyses, such as frequency of each ovule stage based on flower size and sexual behavior, were performed by using the software PASW statistics version 18 (http://www.spss.com/statistics/).

Results

Ovule development and gamete formation in sexual *H. perforatum*

Hypericum perforatum has a flower composed of five sepals and petals surrounding the internal male and female

whorls. The internal tricarpellate syncarpic gynoecium is inserted onto the receptacle above the points of insertion of the outer whorl and the numerous stamens. One single *H. perforatum* ovary yields from 50 to more than 100 ovules, with ovules borne on sporophytic tissues by axile placentation (data not shown).

First developmental stages of the ovule are shown in Fig. 1. As the ovule primordium reaches approximately 15 cells in length, the emerging integument undergoes periclinal division (Fig. 1). Integumentary growth delineates the main funicular, chalazal and nucellar domains within the ovule (Fig. 1). The *Hypericum* ovule is bitegmic as both outer and inner integuments differentiate from the middle region of the proximal–distal axis of the ovule (Figs. 1 and 2). At this stage, the nucellus is about five cells in length and is composed of one epidermal layer, enclosing one to two hypodermal columns of cells (Fig. 1). We found the number of hypodermal cells to be variable between ovules of the same plant, with no obvious correlation with reproductive behavior (Fig. 2c, d).

As the inner integument starts to form, the evident archesporial cell differentiates just beneath the most apical epidermal cell. No intermediate division of the archesporial cell prior to MMC differentiation was observed (Fig. 1). Callose deposition patterns within sexual ovules fully resemble the pattern previously described by Rodkiewicz (1970) for the monosporic Polygonum type of embryo sac formation (Fig. 3b–e). DAB-induced fluorescence is strongly localized at both poles of the MMC, with crescent-like accumulation that finally encompasses the complete internal surface of the cell (Fig. 3b). First meiotic division and cytokinesis lead to marked callose deposition within the middle cell wall (Fig. 3c), and at this time little or no callose is present within the proximal–distal apex of the dyad.

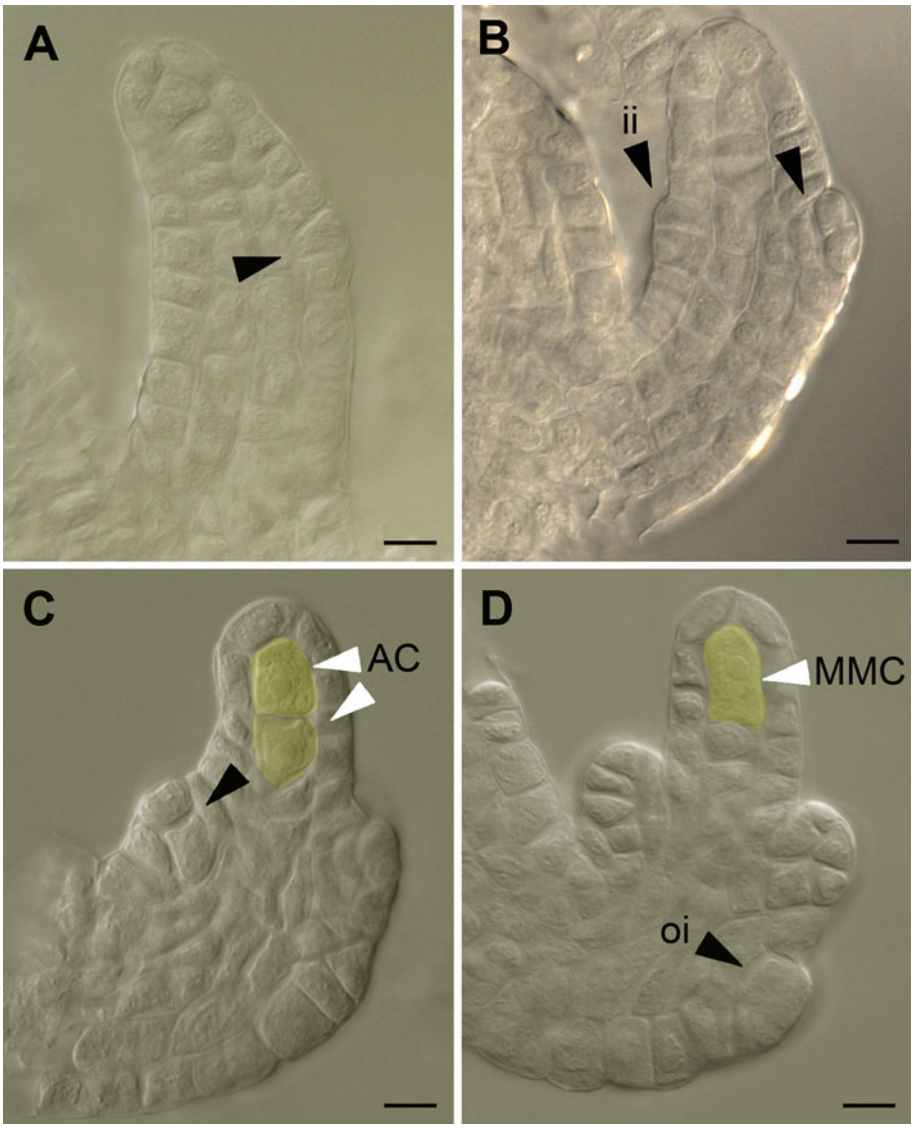

Fig. 1 Early phases of ovule development in sexual and aposporous *H. perforatum* plants. **a** Ovule at the stage of inner integument initiation in the abaxial side (at this stage, the epidermal layer is distinguishable from the internal subepidermal tissue); **b** ovule at the stage of inner integument initiation in the adaxial side (the development of adaxial inner integuments is anticipated with respect to the abaxial side); **c** ovule showing a couple of archesporial cells (*highlighted in yellow*); **d** ovule containing a megaspore mother cell (*highlighted in yellow*). *Black arrowheads* indicate the sites of integument formation. Note that outer integument initiation shortly follows inner integument protrusion. The archesporial cells are located next to the epidermis, with the most micropylar subepidermal cell of the nucellus committed to form the MMC. *ii* inner integument, *oi* outer integument, *AC* archesporial cell, *MMC* megaspore mother cell. *Bars* 17 μm

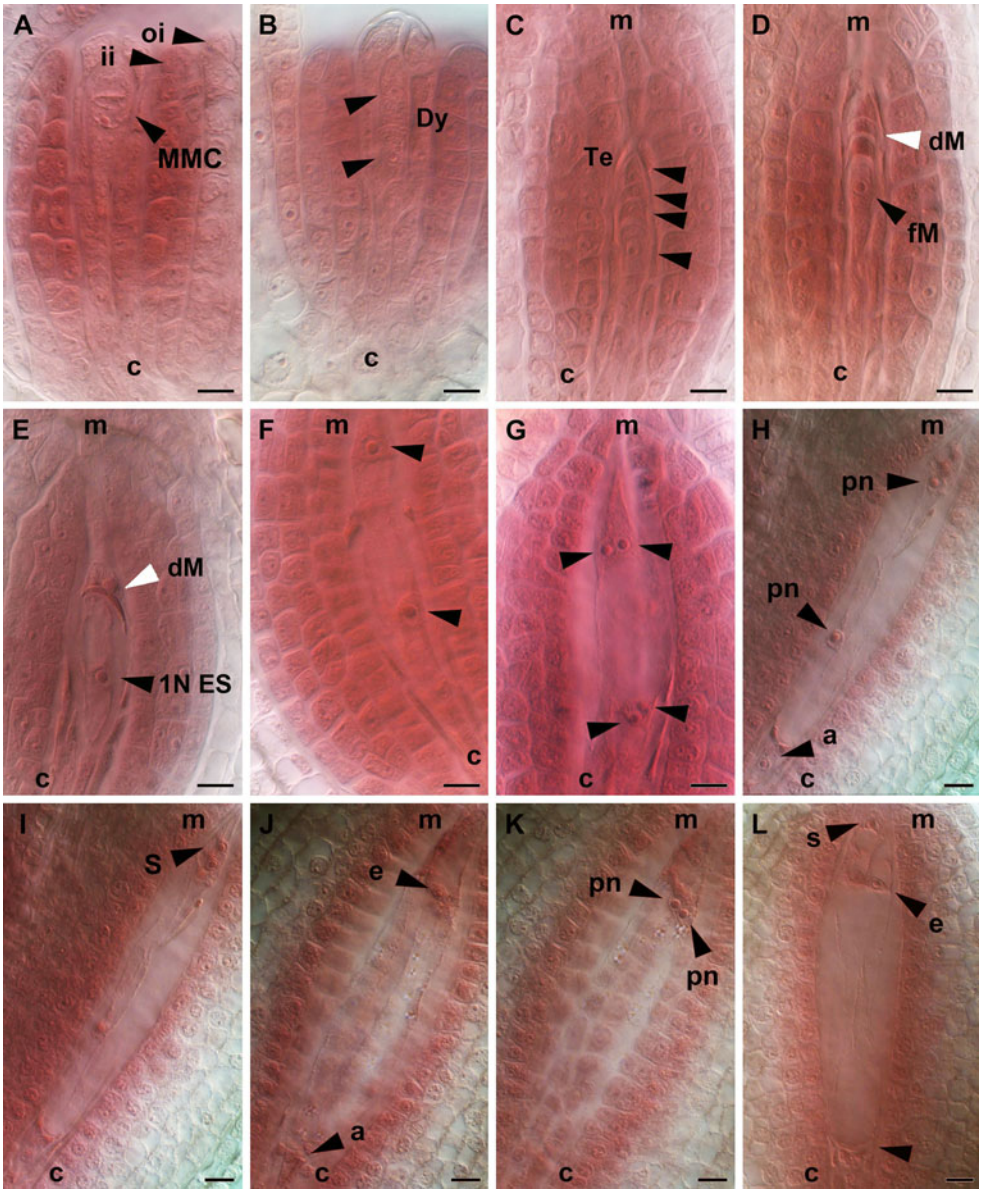

Fig. 2 Megasporogenesis (**a**–**d**) and megagametogenesis (**e**–**l**) progression in sexual *H. perforatum*. For each panel, the micropylar (*m*) and chalazal (*c*) side of the ovules are indicated. **a** Megaspore mother cell (*MMC*); **b** dyad (*Dy*); **c** linear tetrad of megaspores (*Te*); **d** functional megaspore (*fM*) with degenerating megaspores (*dM*). Ovules with a one or multinucleate developing embryo sac (*ES*): **e** 1 N ES; **f** 2 N ES; **g** 4 N ES; **h**–**k** 8 N ES spanning the time point of antipodal degeneration; **l** mature ES, showing degenerated antipodals. Nuclei within megaspores and embryo sacs are marked with *black arrowheads*. *o* outer integument, *ii* inner integument, *il* inner layer, *el* external layer, *pn* polar nuclei, *a* antipodal, *s* synergid, *e* egg cell. *Bars* 8 μm

Callose is furthermore clearly detectable within the young tetrad stage (Fig. 3d, e), strongly accumulating in cell walls of newly formed megaspores. Late tetrads are recognizable from younger ones by the massive accumulation of polysaccharides around all but the functional megaspores. As in *Arabidopsis* and maize, only the most proximal megaspore survives to undergo further development (Fig. 2d, e). The complete degeneration of the most micropylar megaspores is accompanied by the onset of megagametogenesis, in which the enlargement of the functional megaspore gives rise to the one nucleate embryo sac (Fig. 2e).

The first mitotic nuclear division of the one nucleate embryo sac leads to the two nucleate embryo sac (early 2 N ES stage, data not shown). The positioning of the two nuclei within the embryo sac is highly conserved and predictable, as they are always detectable in the proximal and distal sides of the cell. Prior to the second mitotic division, the embryo sac markedly increases in length, almost reaching the most micropylar side of the ovule (late 2 N ES stage; Fig. 2f). The second nuclear division of the proximal and distal nuclei is highly synchronized and results in the formation of a four nucleate embryo sac with two nuclei localized at opposite

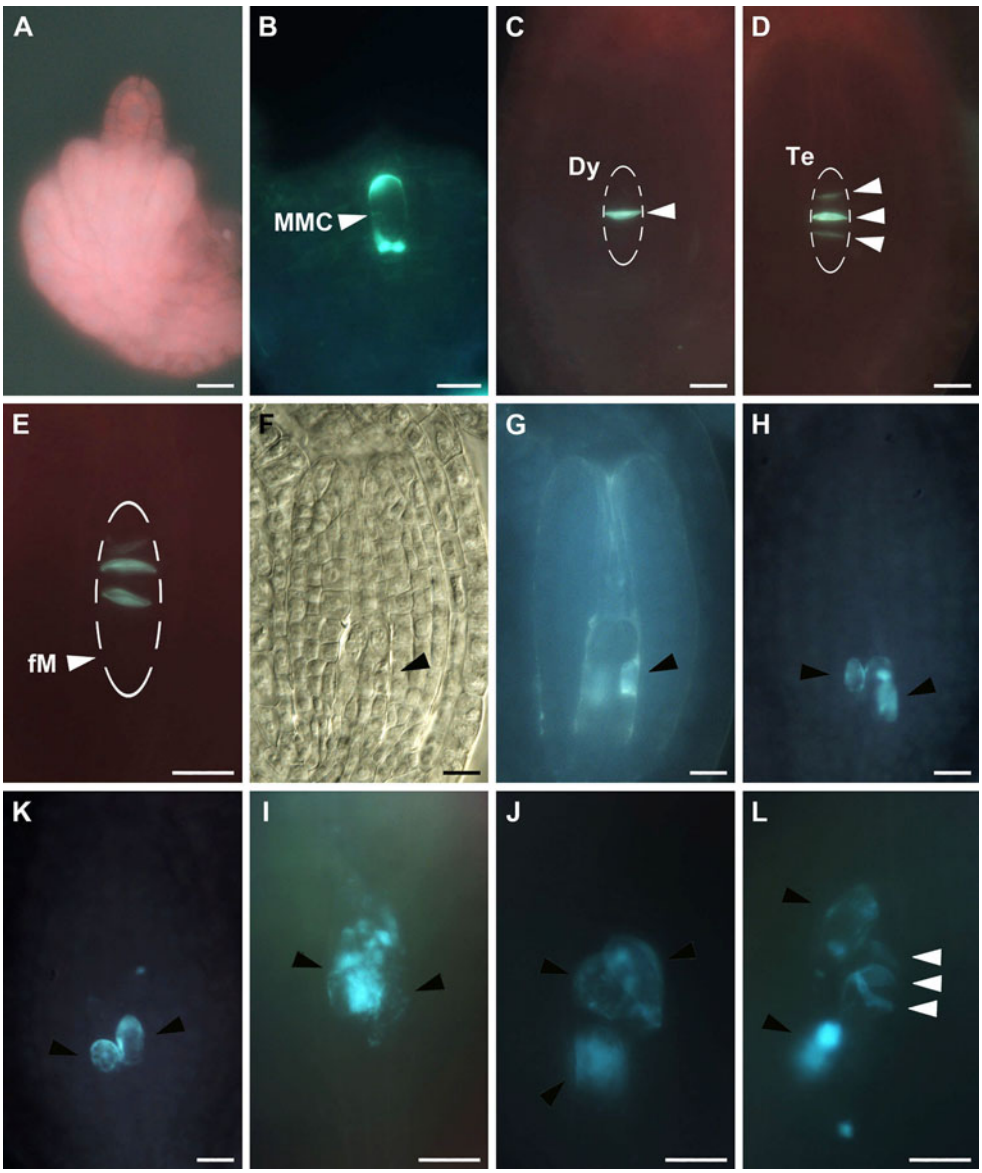

Fig. 3 Callose localization detected by decolorized aniline blue labeling of sexual (**a**–**e**) and aposporous (**f**–**l**) ovules at pre-meiotic and meiotic developmental stages. **a** Pre-meiotic ovule: no callose is deposited within the nucellus; **b** megaspore mother cell (*MMC*); **c** dyad (*Dy*); **d**, **e** linear tetrad of megaspores (*Te*) with a functional megaspore (fM), the middle cell wall is the major site of callose accumulation at this developmental stage. **f**, **g** ovule isolated from an apomitic individual, photographed under normal light (for cell/tissue visualization) and UV light (for callose visualization): fluorescence shows callose deposition boundaries around the embryo sac cavity. **h**–**l** non-conventional sites of callose deposition (panels H and K), with spread or spotted distribution (panels I, J, and L). Note that in addition to sexual-like patterns of callose localization into megaspores, flanking cells resembling aposporic initials also accumulated callose (compare with E–L). *Bars* 13 μm

poles of the cell (Fig. 2g). A precise and conserved pattern of nuclear positioning within the ES is observed at this stage, suggesting that this is under strict control. More specifically, the nuclei are positioned one above the other with respect to the chalazal pole of the micropylar/chalazal axis, while the nuclei generally are located side by side at the micropylar end (Fig. 2g). The third nuclear division closely follows the second one to generate the final eight-nucleated embryo sac (8 N ES; Fig. 2h, i). As cytoplasm and organelle partitioning take place, two antipodals and synergids originate from the most externally localized nucleus, while all other constituents of the mature embryo sac are derived from the more centrally localized nuclei (Fig. 2h). The mature, fully cellularized embryo sac is composed of the three antipodals, a binucleated central cell and the egg cell positioned beneath the two most micropylar synergids (Fig. 2l). Synergids and egg cell are clearly characterized by inverted localization of the large vacuole and nucleus with respect to one another

(Fig. 2l). Indeed, while synergids are typically characterized by a distal nucleus and a proximal vacuole, the egg cell is characterized by the presence of a distally localized vacuole and a proximal cytoplasmic area (Fig. 2l, black arrowheads). Such organization of the egg cell results in the proximity of the large nucleus of the germ cell to the secondary nucleus of the central cell, the latter being distally localized within the large auxiliary cell (Fig. 2l). We observed that degeneration of the antipodal cells always precedes polar nuclei fusion (Fig. 2h, i) and secondary nucleus formation always precedes synergid cell degeneration and fertilization of the embryo sac (Fig. 2j, k).

Aposporous embryo sac induction and development

Significant deviations from the sexual pathway were observed within aposporous ovules. Isolated ovules from apomictic individuals were typically characterized by an archesporial cell that eventually produced a MMC, which apparently mimics the developmental timing observed in sexual individuals. As shown in Fig. 4 (panels b–d), even if megaspore-like enlarged cells seem to be present within the hypodermal layer, meiosis frequently stops at the two to four megaspore stage. Furthermore, if distinguishable from the surrounding cells, such megaspores typically carry a small nucleus and exhibit signs of degeneration (Fig. 4a–c). Moreover, the ovules of apomictic individuals are characterized by novel callose deposition patterns compared to those of sexuals and very rarely show dyads or tetrads (Fig. 3). Furthermore, FCSS analysis confirmed that apomictic individuals retained low frequencies of sexual seed formation (Table 2), and thus the possibility that our embryological observations of dyads and tetrads reflect meiosis rather than aposporous apomeiosis cannot be ruled out.

In contrast to sexual ovules, aposporous ovules are characterized by diffuse fluorescence signals in place of the clearly defined callose deposition normally associated with meiotic progression, and brightly stained single cells were frequently observed in both hypodermal and epidermal areas of the nucellus, where sporogenesis is not likely to take place (Fig. 3). In addition to arrest of megasporogenesis, the number and morphology of cells involved with aposporous seed production deviate from that which is characteristic of normal development (Fig. 4). These cells are clearly recognizable in the apomeiotic embryo sac and share a number of traits: (1) exclusive to apomeiotic ovules; (2) differentiate from the epidermal layer of the nucellus; (3) cell size considerably increased with respect to the neighboring ones; (4) large vacuoles frequently present along both sides of the cell and a dense cytoplasmic middle region and (5) clearly defined large nucleus. It is worth mentioning that older aposporous ovules (i.e., larger ovules isolated from longer flower buds) were frequently characterized by the presence of a large developing coenocyte clearly developing from the same target area of the nucellus. Considering these morphological traits and the apparent ability to escape their conventional cell fate, we defined these cellular types as aposporic initials.

Aposporic initials (AIs) are typically elliptical in shape, frequently drop shaped and clearly distinguishable from the square-shaped neighboring epidermal cells (Fig. 4a–c). Early developmental steps of AIs are characterized by dramatic growth in length and width, and the concomitant displacement of the surrounding, mostly hypodermal, tissues (Fig. 4b, c). Furthermore, the neighboring cells are frequently arrested in development or appear as degenerating megaspores (Fig. 4b–d). Interestingly, the increase in size and particularly in length of the AIs was comparable with that of enlarging sexual embryo sacs, achieving three to four times the length of surrounding cells prior to any nuclear division (compare Figs. 2e and 4c, d). The first nuclear division of the centrally localized nucleus of the AI results in the formation of a binucleate coenocyte, whose nuclei are localized to the apex of the cell in a pattern similar to the sexual early 2 N ES (Fig. 4e). After this nuclear migration, second and third nuclear divisions usually take place within the sac (Fig. 4f–j). Frequently, the second and third divisions seem to be asynchronous and lead to unconventionally nucleated coenocytes when compared to the sexual 4 N and 8 N ES morphologies (compare Figs. 2 and 4).

Two main types of deviation from the developmental pattern of sexual embryo sacs were observed within aposporous coenocytes. First, aposporous embryo sacs may contain an odd number of nuclei, resulting in three, five and nine nucleate cells (Fig. 4f, h, k and l). Second, nuclear positioning within the sac frequently does not resemble the Polygonum type, and results, for instance, in the presence of two to six nuclei in the most micropylar pole of the embryo sac (Fig. 4f–m). While these deviations in nuclear distribution are linked with asynchronous cell division, it is unclear whether this is a cause or consequence. The 4 N ES stage is additionally characterized by a coenocyte that frequently possessed four nuclei localized in the four corners of the embryo sac (Fig. 4g).

The localization pattern of nuclei within the aposporous embryo sac following the third mitotic division frequently differs from that in sexual embryo sacs. However, as cellularization proceeds, the identification of most cell types was possible, considering their position and morphological traits. Normally, one to two antipodal cells are proximally localized in the embryo sac, but they rarely resembled the characteristic triangular morphology observed in sexual ovules (Fig. 4g–j). Furthermore, degeneration of the antipodal cells within aposporous

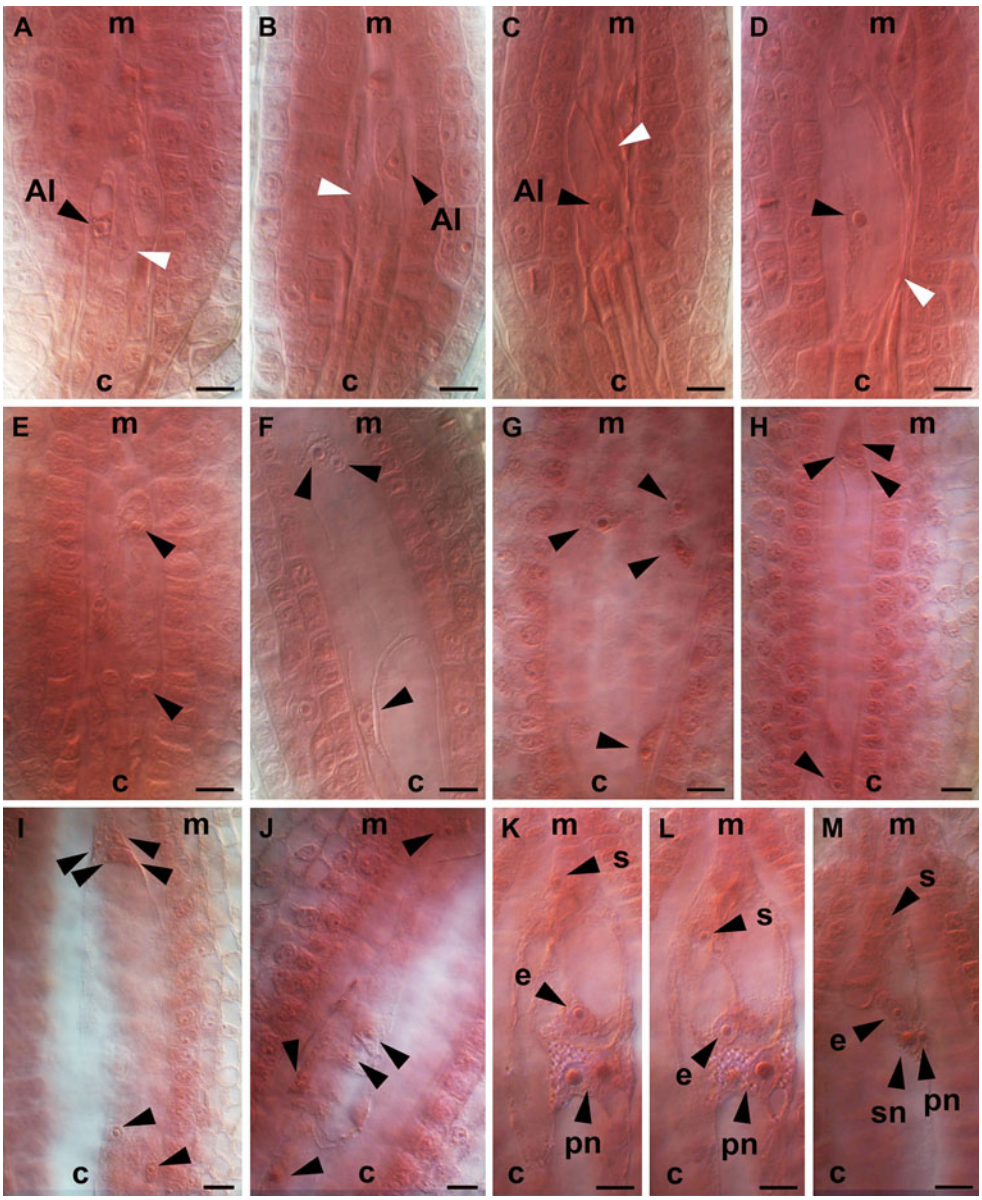

Fig. 4 Embryo sac development within aposporous ovules. The micropylar (*m*) and chalazal (*c*) sides of the ovules are reported for each panel. **a–c** Aposporic initial (*AI*) differentiation and enlargement; **e–j** coenocytic growth of the aposporic initial which finally gives rise to an embryo sac; **k–m** egg cell apparatus with supernumerary cells (**k–l**) or nuclei (**m**). From a to f, the cellular layer in which the aposporic initial differentiates is clearly detectable (*white arrows* indicate the expected location of megaspores, whereas black arrows mark nuclei detectable within coenocytic megagametophytes). *Symbols*: *s* synergid, *e* egg cell, *sn* secondary nucleus, *pn* polar nucleus. *Bars* 8 μm

embryo sacs frequently occurs earlier with respect to the sexual ones. The egg cell is always easily detectable soon after cellularization, and as observed in sexual ovules, it is localized in the most micropylar side of aposporous ovules and is characterized by a pronounced proximal nucleus and a large distal vacuole (Fig. 4k, l). Based on cell morphology and positioning within the embryo sac, ovules bearing multiple egg cells in the same structure were observed in aposporous but not in sexual preparations (Fig. 4k, l). Hence, in the most extreme cases, the embryo sac contains what appears to be degenerating synergids and supernumerary nuclei (Fig. 4m) or cells (Fig. 4k, l). We could not rule out the possibility that eventual supernumerary egg cells are functional. In contrast, synergids are frequently difficult to localize or atypically shaped and appear close to degeneration (Fig. 4j–m).

Apomictic individuals typically have ovules bearing large degenerating cells, and in a few cases, an enormously enlarged nucleus or no nucleus at all, all of which suggesting embryo sac degeneration. One to four AIs were

Table 2 Frequencies of embryo and endosperm genome size ratios observed in different aposporic accessions of *H. perforatum*, and the total number of seeds for which the *C* value (Matzk et al. 2001) was estimated with no ambiguities

Plant	Embryo:endosperm ratios (%)								Total
	2:6	2:8	4:6	4:8	4:10	4:12	4:14	6:10	
H06_1915	–	–	2	–	90	–	–	8	37
H06_2751	–	3	10	3	67	–	–	17	29
H06_2849	3	–	8	–	76	3	–	10	39
H06_2974	–	–	2	–	72	–	2	22	40

recorded within the same nucellus, which eventually led to multiple enlarged coenocytes within the same ovule (Fig. 5). The developmental stages of multiple AIs, when present, were frequently unsynchronized. Moreover, the developmental stages of multiple aposporous embryo sacs suggest a distal–proximal gradient, frequently visualized as the larger coenocyte reaching the micropylar pole, in opposition to newly differentiated AIs enlarging in the chalazal side (Fig. 5). In contrast, no obvious adaxial–abaxial developmental gradient was observed. The formation of multiple AIs within the same ovule further enabled us to restrict the target area of AI differentiation to the epidermal cell layer of the nucellus (Fig. 5).

Synchrony of female gametophyte development

The distribution of embryo sac development stages during flower bud expansion in both sexual and aposporous accessions is shown in Fig. 6. Ovules isolated from sexual and aposporic individuals are characterized by relatively conserved patterns in gametophyte development within the pistil, as little frequency variation was observed among the analyzed pistils (Fig. 6). As expected, aposporous initials were not observed within pistils isolated from sexual accessions, whereas in agreement with the FCSS data, the opposite was true (i.e., functional megaspores were not isolated within ovules from apomictic reproducing accessions).

Progression of ovule development according to bud size is efficiently shown in Fig. 6 by the progressive increase in the frequency of late ovule stages following the expansion of the bud. As an example, a higher frequency of MMC within sexual accession was recorded in 4–5 mm flower buds, FM peaked correspondingly in 6–7 mm flower buds, whereas most of the gametophytes classified as eight-nucleate embryo sac (8 N ES, Fig. 6) were located within the longer buds. According to this data, intermediate developmental stages were localized throughout the diagonal ideally connecting the younger and older developmental stages. Based on this, we could for instance determine that higher probability to isolate an ovule at tetrad stage is within 5 to 6-mm-length flower bud (in a scale ranging from 1 to 12). Similarly, we could estimate that about 90% of meiotic processes were concluded as the flower bud reached 6 mm in length.

It is interesting to point out that ovule frequency distribution in apomictic accessions significantly diverged from sexual accessions over all investigated bud lengths with the only exception of the younger ones. Indeed, this flower stage included mainly MMC, while a low rate of recurrence of AIs was noted.

Surprisingly, the presence of AIs within pistils isolated from known apomictic accessions is distributed over all

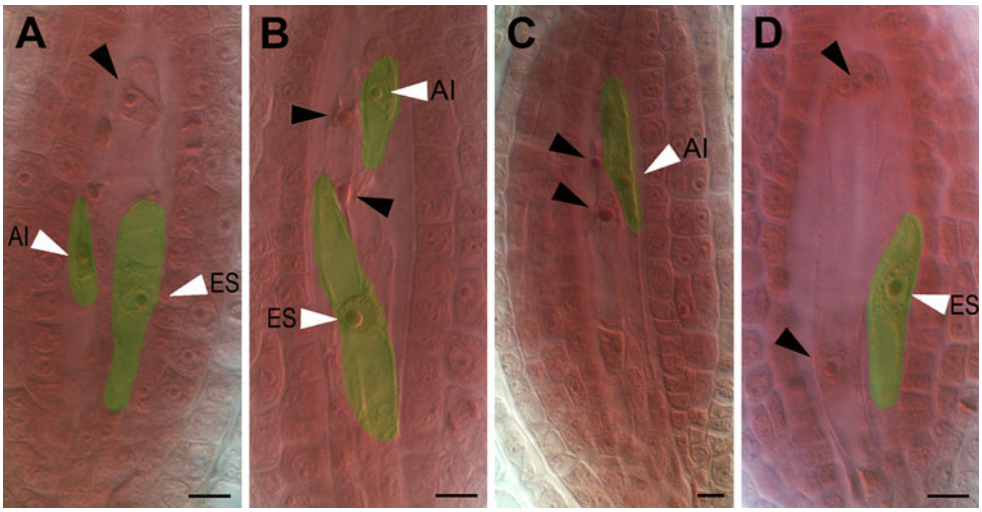

Fig. 5 Ovules of apomictic genotypes, displaying sexual embryo sacs (*ES*) along with aposporous initials (*AI*). **a**, **b** Ovules showing a small aposporic initial and an enlarged one nucleate aposporic embryo sac (*white arrowheads*), together with sexual megaspores (*black arrowheads*). **c**, **d** coexistence of a binucleate or tetranucleate embryo sac and an aposporic initial or aposporic embryo sac within the same ovule (*white arrowheads* indicate aposporic elements, *black arrowheads* point to sexual megaspores or embryo sacs). *Bars* 8 μm

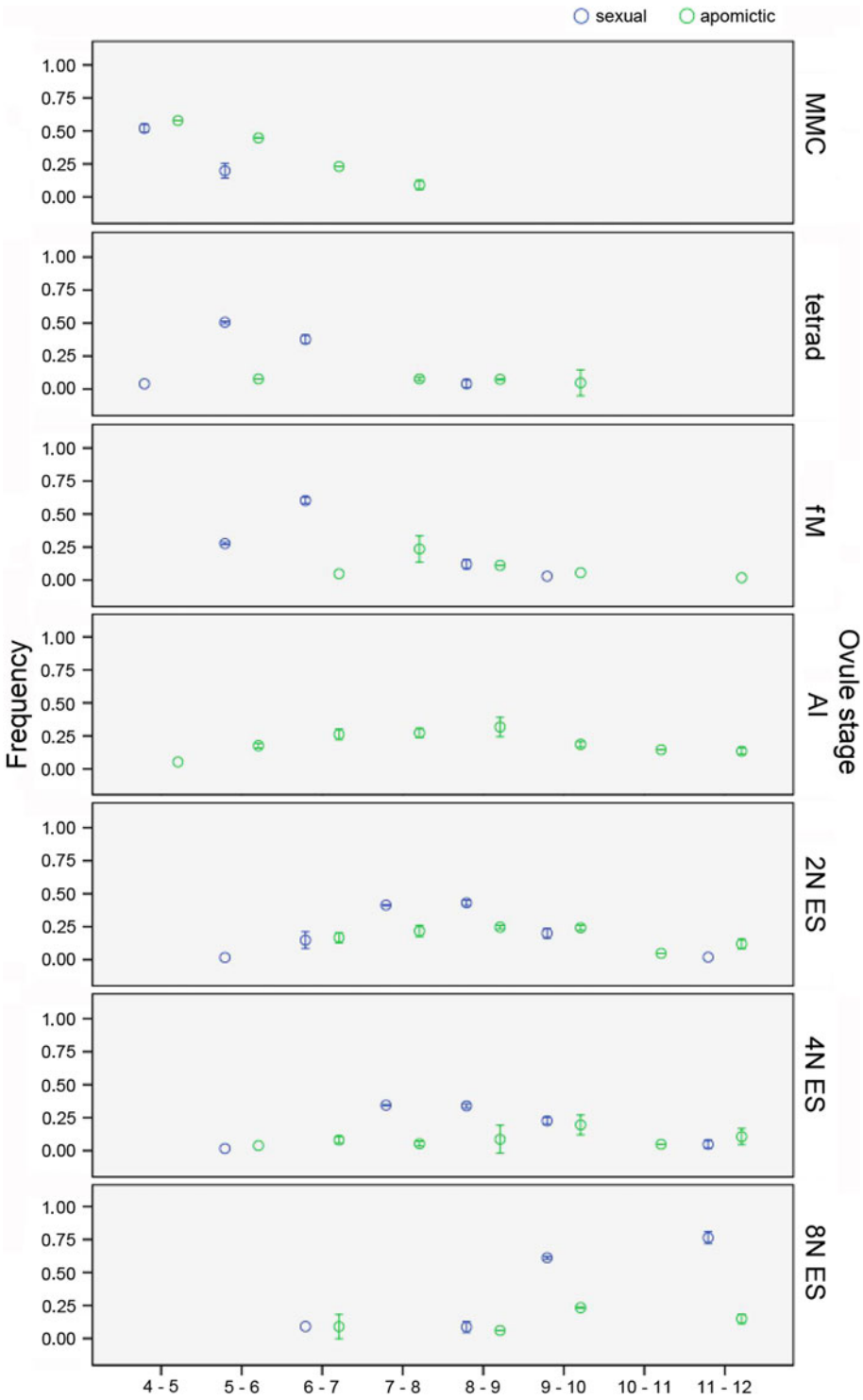

Fig. 6 Statistics on frequency of female sporogenesis and gametogenesis stages observed within dissected developing ovules. *Graphs* represent the calculated frequency (*Y*-axis) for single ovule stages, spanning from MMC to 8 N ES depending on pistil length (*X*-axis). Cytological data for sexual and aposporous individuals are shown as *blue* and *green circles*, respectively. *Symbols*: *MMC* megaspore mother cell, *fM* functional megaspore, *AI* aposporic initial, *N* nuclei, *ES* embryo sac

analyzed samples with a maximum peak located between 6- and 9-mm flower buds. Taking this into account, it is not surprising that later developmental stages such as 2 N ES, 4 N ES and 8 N ES are shifted toward maturity of the flower bud, when compared to the same ovule stages within flowers collected from sexual accessions.

FCSS analyses

Based upon the flow cytometric profiles of single seeds, the four tetraploid (4C) accessions collected from different geographical regions were all determined to be facultative apomictic, with 67–90% of the analyzed seeds per accession having an embryo/endosperm ratio

Table 3 Expected *C* values in seeds originating through sexual and apomictic reproduction

	Egg cell	Central cell	Double fertilization	Fertilization Autonomous endosperm formation	Parthenogenesis Autonomous endosperm formation	Pseudogamy
			Sperm nuclei ($2x - 2x$)	Sperm nuclei ($2x - 0$)	Sperm nuclei ($0 - 0$)	Sperm nuclei ($0 - 2x$)
Meiosis	$2x$	$4x$ ($2x + 2x$)	***4C*:*6C***	4*C*:4*C*	2*C*:4*C*	2*C*:6*C*
	$2x$	$2x$ ($2x + 0$)	4*C*:4*C*	4*C*:2*C*	2*C*:2*C*	2*C*:4*C*
	$2x$	$6x$ ($2x + 2x + 2x$)	4*C*:8*C*	4*C*:6*C*	2*C*:6*C*	2*C*:8*C*
Apospory	$4x$	$8x$ ($4x + 4x$)	6*C*:10C	6*C*:8*C*	***4C*:8*C***	***4C*:10*C***
	$4x$	$4x$ ($4x + 0$)	6*C*:6*C*	6*C*:4*C*	4*C*:4*C*	4*C*:6*C*
	$4x$	$12x$ ($4x + 4x + 4x$)	6*C*:14*C*	6*C*:12*C*	4*C*:12*C*	4*C*:14*C*
			Sexuality		Apomixis	

Haploid genome content (x) is reported for both maternal and paternal gametes and accessory cells. *C* values corresponding to expected and observed ratios for double fertilization, parthenogenesis and pseudogamy are in bold

of 4:10 (Tables 1 and 2). This ratio reflects parthenogenetic development of the unreduced egg cell (4C) and fertilization of the unreduced central cell (8C) with a reduced 2C sperm nucleus (Table 3). Moreover, all analyzed apomictic individuals exhibited low levels of 4:6 embryo/endosperm, which likely demonstrate double fertilization of reduced embryo sacs (Table 2). This ratio (i.e., embryo/endosperm ratio equal to 4:6) likely represents sexual seed production and ranged from 2 to 10% (Table 2). Double fertilization of the unreduced embryo sac, with diploid and reduced sperm nuclei, as demonstrated by a 6:10 embryo/endosperm ratio, was also present in 8–22% of the analyzed seeds (Table 2).

Besides these main patterns of embryo and endosperm formation, a number of low frequency phenotypes were also observed and suggested more complex pathways of embryo sac formation and fertilization (Tables 2 and 3). For example, low frequencies of 4:8 (parthenogenesis and autonomous endosperm formation from an unreduced embryo sac) and 2:6 (parthenogenesis and pseudogamous development of a reduced embryo sac) embryo/endosperm ratios were identified (Table 2). Furthermore, low frequencies of 2:8, 4:12 and 4:14 ratios were observed (Table 2), which could reflect either the formation of trinucleated central cells or the production of functional unreduced pollen grains (Table 3). If trinucleated central cell formation was the case, the maternal/paternal genome balance within the endosperm would equal 6C:2C, 12C:0C and 12C:2C (Table 3), respectively, for the three embryo/endosperm abovementioned ratios. Alternatively, unreduced tetraploid and hexaploid pollen grain formation could also explain the observed genome ratios. Double fertilization of either reduced or unreduced embryo sacs by unreduced pollen grains was never observed.

Discussion

Hypericum perforatum is characterized by quantitative variation in reproductive mode, as demonstrated by the cytological and FCSS investigations here, in addition to previous works (Matzk et al. 2001, recently reviewed by Barcaccia et al. 2007). The multiple pathways of seed formation in tetraploid apomictic individuals are reflected in variable embryo and endosperm genome ratios, which range from 2:8 (for reduced parthenogenic, pseudogamous development) to 4:14 (for unreduced parthenogenic, pseudogamous development). We furthermore identified significant levels of both autonomous endosperm formation (i.e., 4:8) and double fertilization of both egg cell and central cell (i.e., 6:10), as was also reported by Matzk et al. (2001). These deviations demonstrate relaxation in the constraints on endosperm balance number (EBN; Johnston et al. 1980) which is characteristic of sexual angiosperms. These data are consistent with deviations from the strict 2m:1p endosperm ratio in other apomictic taxa, including *Boechera* (Voigt et al. 2007), *Tripsacum*, *Paspalum* and *Hieracium* (reviewed by Koltunow and Grossniklaus 2003). Interestingly, the association of autonomous endosperm formation with egg cell fertilization was never observed here. However, it might be possible that exclusive fertilization of the egg cell does occur, but perturbation of the embryo/endosperm ratio leads to selective abortion of these ovules. The nutritional and physiological role of endosperm with respect to the developing embryo might account for this latter hypothesis, since low ploidy of the endosperm might result in hypotrophic growth and prevent the endosperm from acquiring sufficient resources to sustain itself or the embryo (Scott et al. 1998).

These cytological data might be considered as due update of *Hypericum* ovule development by means of tissue staining-clearing and high-resolution imaging. The original work was

reported over 60 years ago by the pioneer publications of Noack (1939, 1941). Data presented here would be well complemented by high-throughput and -omics applications now available. The sexual ovule is anatropous, bitegmic (i.e., with two integuments) and tenuinucellate and encloses at maturity a monosporic, Polygonum-type embryo sac. The aposporous ovule retains all major morphological characteristics reported herein but fails to develop a reduced embryo sac. In contrast to the sexual pathway, the aposporous embryo sac develops through a series of free nuclear divisions from a single sporophytic cell, which belongs to the epidermal cell layer of the nucellus. Our observations imply that the major developmental features characteristic of aposporous ovule formation include: (1) misexpression of the meiotic program, (2) failure or delay in degeneration of the nucellus epidermal layer, (3) AI differentiation and (4) development into an alternative coenocytic embryo sac. Furthermore, (5) low frequencies of sexual developing ovules are retained within the aposporous ovary. This finding is partially in contrast to the data illustrated by Noack in his publications dated 1939 and 1941, in which aposporous initials were reported to differentiate from the hypodermal cell layer of the nucellus. Indeed, while the aposporous nature of *H. perforatum* and the general importance of the nucellus in AI differentiation are confirmed, our results rather demonstrate that most AIs differentiate from the external cell layer of the nucellus.

The importance of AI positioning with respect to the site of differentiation of the meiotic products has been reported for several aposporous species. This is the case of *Hieracium*, as one to many AIs were reported to differentiate in close connection with the megaspores in *H. piloselloides* and *H. aurantiacum* (Koltunow et al. 1998). Moreover, aposporous gametophyte development is influenced by AI mispositioning resulting from the *loa1* mutation (Okada et al. 2007). Similarly, the correct positioning of AIs in *Hypericum* ovules seems to be necessary for further development, as no AIs or embryo sacs were ever detected more distantly from the site of megasporogenesis within the nucellus. Since both MMCs and AIs originate from the same site of differentiation, the nucellus, it is likely that the two processes depend on the expression of specific factors restricted to this area of the ovule. This is coherent with the widespread idea in the embryologist community that technically the nucellus is the angiosperm megasporangium, the implication of which is that nucellar cells are by nature more capable developmentally of reproductive development. Furthermore, the fact that megasporogenesis is limited to the hypodermal inner area and never occurs in the epidermal cell layer, where aposporous initials are confined, suggests an additional regional level of regulation within the nucellus background.

It is generally recognized that callose deposition during megasporogenesis progression might play a role in isolation of the MMC from surrounding tissues, in addition to the regulation of the fate of meiotically derived megaspores, by physically limiting symplastic communication with adjacent cells (Rodkiewicz 1970; Haig 1990). It is well known that the pattern of callose deposition in ovules of sexual species is not conserved in apomeiotic pathways, as has been shown in *Elymus rectisetus* (Carman et al. 1991), *Hieracium* spp. (Tucker et al. 2001) *Poa pratensis* (Naumova et al. 1993), *Tripsacum dactyloides* (Leblanc et al. 1993) and *Medicago falcata* (Barcaccia et al. 1996), where meiosis is bypassed or disturbed. In this species, the lack of callose accumulation has been reported for both AIs (Peel et al. 1997; Tucker et al. 2001) and MMCs undergoing diplosporic development (Carman et al. 1991). Within aposporic ovules of *H. perforatum,* callose deposition is frequently lacking or follows unconventional patterns. Even if we cannot rule out the possibility that the alteration in callose deposition observed at the stage of AI formation is not the cause of megaspore degeneration, but rather a consequence, it is reasonable to conclude that changes in callose accumulation reflect a deregulation in normal cell-to-cell communication. Thus, it is likely that developing megaspores either directly or indirectly regulate epidermal layer proliferation whereby apomeiosis leads to abnormal signaling between closely neighboring cells.

Aposporous initials do not divide in a meiotic pattern but do so mitotically to occupy much of the area enclosed by the two integuments. Despite the evidence of several features shared by both aposporic and sexual embryo sacs, a number of peculiarities in terms of number and position of nuclei in the female gametophyte characterize aposporous ovules. In addition to differences in cell shape and developmental timing, the main differences observed between sexual and aposporous embryo sacs include the number of nuclei and the organization of the embryo sac following cellularization. Nuclear divisions within the embryo sac were frequently asynchronous, leading to unconventional numbers of nuclei that were mispositioned within the same coenocytic structure. Although marker lines are not available in *H. perforatum* and elegant demonstration of cell identity of embryo sac cell components is now rather an easy task, the presence of supernumerary nuclei within the central cell and degeneration of synergids prior to fertilization were demonstrated. Similarly, additional egg cells appeared to be present in aposporic embryo sacs based on cell morphology, positioning and organelle localization within the cell. Synergid degeneration could be interpreted as a physical barrier against fertilization, and multinucleated central cell formation might be particularly interesting with respect to autonomous endosperm formation and parthenogenesis. Our FCSS analyses clearly indicate that fully developed aposporic embryo sacs might bear both a functional egg and a central cell apparatus, as the products of both their fertilization were detected.

Recent publications support the hypothesis that deviation of the fate of cells enclosed in the aposporic embryo sac might be related to mispositioning of nuclei within the embryo sac, prior to cellularization. If this holds true, the characterization of *Arabidopsis* gametophytic mutations such as *eostre* (Pagnussat et al. 2007) and *lachesis* (Groß-Hardt et al. 2007) might help elucidate gametophyte development in *Hypericum*, for example whether apospory involves misregulation of the above-mentioned genes. In this light, it is particularly interesting that specification of cell fate within the *Arabidopsis* embryo sac appears to rely on a position-based mechanism, as the switch from synergid to egg cell is accompanied by mispositioning of the nucleus during early developmental stages (Pagnussat et al. 2007). Similarly, the auxiliary and gametic cell fates within the embryo sac of *Arabidopsis* were recently reported to be affected in the *lachesis* mutant (Groß-Hardt et al. 2007), in which functional supernumerary egg cells differentiate from accessory cells, pointing to a mechanism that prevents accessory cells from adopting gametic cell fate.

Concluding remarks

The elevated variation in aposporic gametophyte development (relative to sexual ones; see Figs. 2, 3 and 6 and Table 2) could reflect stochastic processes, for example perturbations to signaling pathways in the ovule (Okada et al. 2007), or mutation accumulation in independently derived apomictic clones (Koltunow 1993). The two processes might lead to the developmental delay observed in older apomictic ovules, with respect to the sexual counterparts. Similarly, stochastic gametophyte development has been hypothesized in aposporous *Hieracium aurantiacum* (Koltunow et al. 1998), where one to multiple aposporic initials were demonstrated to form and grow without any precise developmental patterns.

Based on the cytological data, we hypothesize that the AI could be an epidermal cell that re-enters the cell cycle to undergo mitotic division, a process that could be influenced by the specific positioning of single cells within the ovule. This idea is coherent with the data recently published by Olmedo-Monfil et al. (2010) in which the role of the protein ARGONAUTE 9 (AGO9) in controlling the formation of female gametes by restricting the specification of gametophyte precursors was demonstrated. In the context of aposporous apomixis, it is interesting that mutation in AGO9 leads to the differentiation of multiple germinal cells that are able to initiate gametogenesis (Olmedo-Monfil et al. 2010). As a consequence, the possibility that apomeiosis would induce one or more of the surrounding sporophytic cells to escape their fate and divide might not be ruled out. If this holds true, the interaction with surrounding structures is likely to be fundamental for the development of the aposporic embryo sac. Moreover, since apospory demonstrates that an embryo sac can originate from a sporophytic cell, epigenetic mechanisms specific to the haploid functional megaspore may not be critical for embryo sac development. Further, as the sexual tetraploids used here were generated from sexual diploid accessions (Table 1), gene copy number or DNA quantity alone are unlikely candidates to explain the differences between sexual and apomictic gametophyte formation. Alternatively, it seems more reasonable that factors required for both aposporic and sexual gametophyte development may be modulated by some regulative elements localized in hypodermal and epidermal nucellar cell domains.

Seed DNA content analysis by FCSS represents a powerful tool for shedding light on the complex fertilization scenarios that take place in *H. perforatum,* where both reduced and unreduced male and female gametes can be produced even by the same genotype. Together with our detailed cytohistological analyses of sexual and aposporic cellular components and developmental patterns, these data provide important observations that will guide subsequent high-throughput experiments into the genetic control and molecular regulation of facultative apomixis in *H. perforatum*.

Acknowledgments Thanks are due to Dr. I. Schubert for his valuable comments on the manuscript. We thank the apomixis research group for enlightening discussions and technical support, and J. Maron (University of Montana, Missoula) for having kindly supplied seed stocks. Authors wish to thank also the anonymous reviewers for their constructive critics and suggestions on the manuscript.

References

Albertini E, Barcaccia G, Porceddu A, Sorbolini S, Falcinelli M (2001) Mode of reproduction is detected by Parth1 and Sex1 SCAR markers in a wide range of facultative apomictic Kentucky bluegrass varieties. Mol Breed 7:293–300

Barcaccia G, Mazzucato A, Falcinelli M, Veronesi F (1996) Callose localization in cell walls during meiotic and apomeiotic megasporogenesis in diploid alfalfa (*Medicago* spp.). Caryologia 49:45–56

Barcaccia G, Mazzucato A, Albertini E, Zethof J, Gerats A, Pezzotti P, Falcinelli M (1998) Inheritance of parthenogenesis in *Poa pratensis* L.: auxin test and AFLP linkage analyses support monogenic control. Theor Appl Genet 97:74–82

Barcaccia G, Varotto S, Meneghetti S, Albertini E, Porceddu A, Parrini P, Lucchin M (2001) Analysis of gene expression during flowering in apomeiotic mutants of *Medicago* spp.: cloning of ESTs and candidate genes for 2n eggs. Sex Plant Reprod 14:233–238

Barcaccia G, Bäumlein H, Sharbel TF (2007) Apomixis in St. John's Wort (*Hypericum perforatum*): an overview and glimpse towards the future. In: Hoerandl E, Grossniklauss U, Van Dijk P, Sharbel TF (eds) Apomixis: evolution, mechanisms and perspectives. International Association for Plant Taxonomy, Koeltz Scientific Books, Koenigstein, pp 259–280

Bennett MD, Smith JB (1976) Nuclear DNA amounts in angiosperms. Philos Trans R Soc Lond B 274:227–274

Bicknell RA, Koltunow AM (2004) Understanding apomixis: recent advances and remaining conundrums. Plant Cell 16(Suppl.): S228–245

Carman JG, Crane CF, Riera-Lizarazu O (1991) Comparative histology of cell walls during meiotic and apomeiotic megasporogenesis in two hexaploid Australasian *Elymus* species. Crop Sci 31:1527–1532

Christensen CA, King EJ, Jordan JR, Drews GN (1997) Megagametogenesis in *Arabidopsis* wild type and the *Gf* mutant. Sex Plant Reprod 10:49–64

Davis GL (1966) Systematic embryology of the angiosperms. Wiley, New York

Groß-Hardt R, Kägi C, Baumann N, Moore JM, Baskar R, Gagliano W, Jürgens G, Grossniklaus U (2007) LACHESIS restricts gametic cell fate in the female gametophyte of *Arabidopsis*. PLoS Biol 5:e47

Gustine DL, Sherwood RT (1997) Apospory-linked molecular markers in buffelgrass. Crop Sci 37:947–951

Haig D (1990) New perspectives on the angiosperm female gametophyte. Bot Rev 56:236–275

Huang B-Q, Sheridan WF (1994) Female gametophyte development in maize: microtubular organization and embryo sac polarity. Plant Cell 6:845–861

Johnston SA, den Nijs TPM, Peloquin SJ, Hanneman RE (1980) The significance of genetic balance to endosperm development in interspecific crosses. Theor Appl Genet 57:5–9

Koltunow AM (1993) Apomixis: embryo sacs and embryos formed without meiosis or fertilization in ovules. Plant Cell 5(10):1425–1437

Koltunow AM, Grossniklaus U (2003) Apomixis: a developmental perspective. Annu Rev Plant Biol 54:547–574

Koltunow AM, Johnson SD, Bicknell RA (1998) Sexual and apomictic development in *Hieracium*. Sex Plant Reprod 11:213–230

Koperdakova J, Brutovska R, Cellarova E (2004) Reproduction pathway analysis of several *Hypericum perforatum* L. somaclonal families. Hereditas 140:34–41

Leblanc O, Peel MD, Carman JG, Savidan Y (1993) Megasporogenesis in sexual and apomictic *Trypsacum* species using interference contrasts and fluorescence. Apomixis Newslett 6:14–17

Mansfield SG, Briarty LG, Erni S (1991) Early embryogenesis in *Arabidopsis thaliana*. I. The mature embryo sac. Can J Bot 69:447–460

Mártonfi P, Brutovská R, Cellárová E, Repcák M (1996a) Apomixis and hybridity in *Hypericum perforatum*. Folia Geobot Phytotax 31:389–396

Mártonfi P, Repcák M, Mihoková L (1996b) *Hypericum maculatum* subsp. *Maculatum* × *H. perforatum* (Hypericaceae): corroboration of natural hybridization in *Hypericum* by secondary metabolite analysis. Folia Geobot Phytotax 31:245–250

Matzk F (1991) New efforts to overcome apomixis in *Poa pratensis* L. Euphytica 55:65–72

Matzk F, Meister A, Brutovská R, Schubert I (2001) Reconstruction of reproductive diversity in *Hypericum perforatum* L. opens novel strategies to manage apomixis. Plant J 26:275–282

Mogie M (1992) The evolution of asexual reproduction in plants. Chapman & Hall, London (UK)

Naumova T, Den Nijs APM, Willemse MTM (1993) Quantitative analysis of aposporous parthenogenesis in *Poa pratensis* genotypes. Acta Bot Neerl 42:299–312

Noack KL (1939) Über Hypericum- Kreuzungen VI: Fortpflanzungsverhältnisse und bastarde von Hypericum perforatumL. Z Indukt Abstamm Vererbungsl 76:569–601

Noack KL (1941) Geschlechtsverlust und Bastardierung beim Johanniskraut. Forsch Fortschr 17:13–15

Nogler GA (1984) Gametophytic apomixis. In: Johri BM (ed) Embryology of angiosperms. Springer, New York, pp 475–518

Okada T, Catanach AS, Johnson SD, Bicknell RA, Koltunow AM (2007) An *Hieracium* mutant, *loss of apomeiosis 1* (*loa1*) is defective in the initiation of apomixis. Sex Plant Reprod 20:199–211

Olmedo-Monfil V, Durán-Figueroa N, Arteaga-Vázquez M, Demesa-Arévalo E, Autran D, Grimanelli D, Slotkin RK, Martienssen RA, Vielle-Calzada JP (2010) Control of female gamete formation by a small RNA pathway in *Arabidopsis*. Nature 464:628–634

Ozias-Akins P, Lubbers EL, Hanna WW, McNay JW (1993) Transmission of the apomictic mode of reproduction in *Pennisetum*: coinheritance of the trait and molecular markers. Theor Appl Genet 85:632–638

Ozias-Akins P, Roche D, Hanna WW (1998) Tight clustering and hemizygosity of apomixis-linked molecular markers in *Pennisetum squamulatum* implies genetic control of apospory by a divergent locus which may have no allelic form in sexual genotypes. Proc Natl Acad Sci USA 95:5127–5132

Pagnussat GC, Yu HJ, Sundaresan V (2007) Cell fate switch of synergid to egg cell in Arabidopsis *eostre* mutant embryo sacs arises from misexpression of the BEL1-like homeodomain gene BLH. Plant Cell 19:3578–3592

Peel MD, Carman JG, Leblanc O (1997) Megasporocyte callose in apomictic buffelgrass, Kentucky bluegrass, *Pennisetum squamulatum* Fresen, *Tripsacum* L., and weeping lovegrass. Crop Sci 37:724–732

Pessino SC, Ortiz J, Leblanc O, do Valle CB, Hayward MD (1997) Identification of a maize linkage group related to apomixis in *Brachiaria*. Theor Appl Genet 94:439–444

Robinson-Beers K, Pruitt RE, Gasser CS (1992) Ovule development in wild-type *Arabidopsis* and two female-sterile mutants. Plant Cell 4:1237–1249

Robson NKB (2002) Studies in the genus *Hypericum* L. (Guttiferae) 4(2). Section 9. *Hypericum sensu latu* (part 2): subsection 1. *Hypericum* series 1. *Hypericum*. Bull Nat Hist Mus Lond (Bot) 32:61–123

Roche D, Cong P, Chen ZB, Hanna WW, Gustine DL, Sherwood RT, Ozias-Akins P (1999) An apospory-specific genomic region is conserved between buffelgrass (*Cenchrus ciliaris* L.) and *Pennisetum squamulatum* Fresen. Plant J 19:203–208

Rodkiewicz B (1970) Callose in cell walls during megasporogenesis in angiosperms. Planta 93:39–47

Schneitz K, Hülskamp M, Pruitt RE (1995) Wild-type ovule development in *Arabidopsis thaliana*: a light microscope study of cleared whole-mount tissue. Plant J 7:731–749

Scott RJ, Spielman M, Bailey J, Dickinson HG (1998) Parent-of-origin effects on seed development in *Arabidopsis thaliana*. Development 125:3329–3341

Sheridan WF, Golubeva EA, Abrhamova LI, Golubovskaya IN (1999) The *mac1* mutation alters the developmental fate of the hypodermal cells and their cellular progeny in the maize anther. Genetics 153:933–941

Smyth DR, Bowman JL, Meyerowitz EM (1990) Early flower development in *Arabidopsis*. Plant Cell 2:755–767

Stelly DM, Peloquin SJ, Palmer RG, Crane CF (1984) Mayer's hemalum-methyl salycilate: a stain-clearing technique for observations within whole ovules. Stain Technol 59:155–161

Tucker MR, Paech NA, Willemse MTM, Koltunow AM (2001) Dynamics of callose deposition and ß-1, 3-glucanase expression during reproductive events in sexual and apomictic Hieracium. Planta 212:487–498

Voigt M-L, Melzer M, Rutten T, Mitchell-Olds T, Sharbel TF (2007) Gametogenesis in the apomictic *Boechera holboellii* complex: the male perspective. In: Hoerandl E, Grossniklauss U, Van Dijk P,

Sharbel TF (eds) Apomixis: evolution, mechanisms and perspectives. International Association for Plant Taxonomy, Koeltz Scientific Books, Koenigstein, pp 235–258

Worrall D, Hird DL, Hodge R, Paul W, Draper J, Scott R (1992) Premature dissolution of the microsporocyte callose wall causes male sterility in transgenic tobacco. Plant Cell 4(7):759–771